Chapter 10
Retractable Rod Vortex Generator

Tomasz Lewandowski

10.1 Introduction

Growing aerodynamic loads of turbine, aircraft, wind turbine, and helicopter rotor blades increase the possibility of flow separation near the surfaces of those elements. In such situations it is necessary to use flow control methods to improve their aerodynamic performance by, for example, reducing aerodynamic drag, increasing lift force, improving heat exchange, and/or reducing noise. We distinguish between active and passive flow control methods. The passive methods include: fixed Gurney Flaps, vortex generators (VG), perforated plates over a cavity, and geometrical shape modification (Flaszynski and Tejero 2013; Doerffer and Szulc 2011; Barakos 2010). All these methods modify the flow without external energy. The active techniques, which require additional energy input, include: synthetic jets, steady suction or blowing, and active Gurney Flaps (Tang et al. 2014; Pastrikakis 2015). The active control methods can be divided into permanently set devices and controlled devices, the latter based on sensors or a control system.

RrVG is a retractable rod, which is placed on the airfoil to influence reenergizing of the boundary layer on a moving airfoil (flow control). Vortex generators are most often used to delay flow separation. To accomplish this, they are often placed on the external surfaces of vehicles and wind turbine blades. It should be noted that the rod vortex generator presented in the literature (Flaszynski and Tejero 2013) is a fixed type vortex generator (passive method). The use of retractable rod vortex generator (RrVG) with a control system (control signal) allows to activate it during the motion of the airfoil only in specified moments, which is its main advantage. The objective of the proposed system is its location on the helicopter main rotor

T. Lewandowski (✉)
Institute of Fluid-Flow Machinery Polish Academy of Sciences,
Fiszera 14 St, Gdansk, 80-231, Poland
e-mail: tomasz.lewandowski@imp.gda.pl

P. Doerffer et al. (eds.), *Recent Progress in Flow Control for Practical Flows*,
DOI 10.1007/978-3-319-50568-8_10

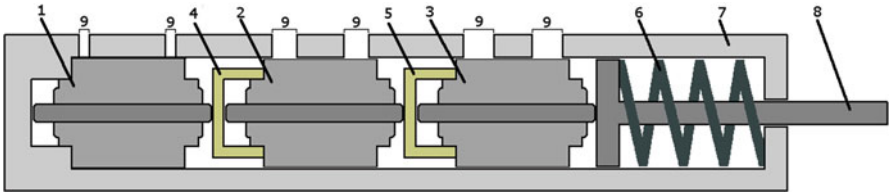

Fig. 10.1 RrVG system—cascade model

blades (Tejero et al. 2014). When constructing this element the knowledge about the structure of the fluid flow and the system control is required. Based on experiments and CFD simulations we should define the best position of RrVG on the blade in relation to the rotor axis, the best angle in relation to the main flow, and the activation moment. Another issue to be decided upon when constructing this system is the choice of the actuator element. It must be appropriately fast and has sufficient deflection.

The LMS software allows to perform a wide range of numerical simulations without the requirement of experiments in the design phase. It allows to simulate the complex system for different frequencies of action, positions, and materials performance of individual elements (parametric study).

10.1.1 Overall Description of the Model

The proposed RrVG system consists of a cascade of several elements. This is due to limitations (dimension and maximum movements) of system elements—actuators. The RrVG model is based on electromechanical components. Figure 10.1 shows the sketch cascade model of the RrVG system.

The designed RrVG system consists of three electromechanical actuators (numbered: 1, 2, 3), two connectors (4, 5), spring (6), retractable rod (8), frame (7), and connection points (9). The principle of work of the system is easy. The body of actuator 1 is clamped to the frame 7. Actuators 2 and 3 are moved by actuator (1), but they move with respect to each other. Actuators (2, 3) move the next elements. The bodies of the actuators (2, 3) are moved by connectors (4, 5). The maximum displacement of the rod (8) is equal to the sum of strokes of all actuators. The task of the spring (6) is to move back the rod. Such a type of design (a cascade) allows relatively easy reconstruction of the system when it is necessary to increase the rod displacement (in order to control the flow with thicker boundary layer). The proposed design is based on existing and easily available elements. Cascade elements for given input signals have been designed and simulated in LMS software. Simulations of cascade system operation were designed to fit and optimize the control system. The response time (activation time) and the total deflection of the rod are analyzed in the chapter depending on the assumed frictional forces and the masses of the system elements.

10.1.2 Numerical Tools

LMS Imagine Lab AMESim is an integrated simulation platform for multi-domain mechatronic systems simulation. LMS Imagine Lab AMESim offers engineers an integrated simulation platform to accurately predict the multidisciplinary performance of intelligent systems and enables you to model, simulate, and analyze multi-domain controlled systems and offers plant modeling capabilities to connect to controls design helping you assess and validate control strategies. To create a system simulation model in LMS Imagine Lab AMESim, you simply access one of the numerous LMS AMESim libraries of predefined and validated components from different physical domains (such as fluid, thermal, mechanical, electromechanical, and powertrain). All simulation library components are completely validated to guarantee the accuracy and reliability of the simulation. By selecting the required validated component from the related library, you avoid creating your own complicated code (Siemens nd).

LMS Virtual Lab (VL) is an integrated suite of 3D FE and multibody simulation software which simulates and optimizes the performance of mechanical systems for structural integrity, noise and vibration, system dynamics, and durability. LMS Virtual.Lab Motion which is part of LMS Virtual.Lab software allows you to investigate the kinematic behavior of systems – including flexible components and controllers – and to design optimally for durability performance (Siemens nd).

10.2 The BLMM Actuator

The electromechanical actuator BLMM (Bistable Linear Moving Magnet) (Fig. 10.2) is offered by CEDRAT Technologies (CEDRAT nd) which was the partner in the IMESCON project. Its main parameters are as follows: stroke of slider 0.62 mm, commutation time 0.0017 ms, total mass 1.1 g, and mass of slider 0.076 g.

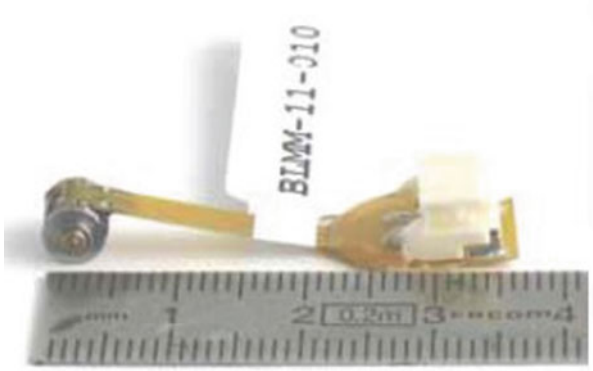

Fig. 10.2 BLMM actuator (CEDRAT nd)

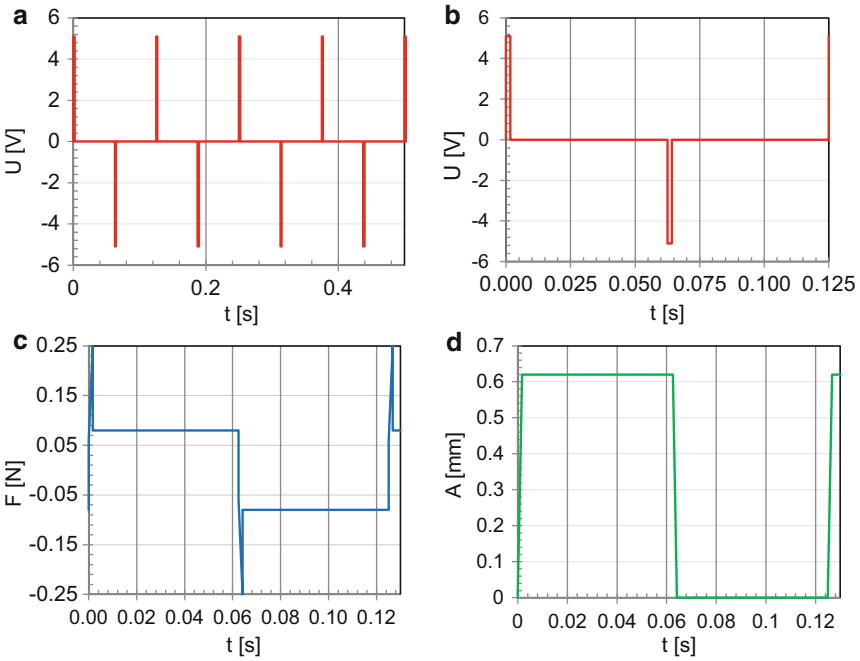

Fig. 10.3 Input and output signals for frequency 8 Hz, (**a**,**b**) voltage input signal, (**b**) force output signal, and (**d**) displacement of the slider

It makes use of a permanent magnet moving between two opposite electromagnets. BLMMs are miniature actuators, a feature which is especially attractive when a small-sized actuator is needed. The main advantages of the BLMM1 actuator are: small size, low power consumption, and fast and easy control. Input and output signals for a single actuator are presented in Fig. 10.3. The signals were determined based on manufacturer's specifications for frequency of 8 Hz. Figure 10.3a, b shows the voltage input signals in which the width of the actuation peak is 0.0017 s (commutation time).

Figure 10.3c presents the force output signal and Fig. 10.3d presents the displacement of the slider (moving part of the actuator). These signals are ideal signals for the unloaded element. Simulations have indicated the need for individual control of each actuator in the cascade.

10.3 Material Description and Friction Force

The outer body of the actuator is made of steel. Aluminum has been selected as the material of the moving elements (connectors and rod), and steel has been selected

Table 10.1 Parameters of materials

Material properties	Aluminum	Steel
Density	2710 kg/m^3	7860 kg/m^3
Young's modulus	7e + 10 Pa	2e + 11 Pa
Poisson's ratio	0.346	0.266
Thermal expansion	2.36e − 05 K/deg	1.17e − 05 K/deg
Yield strength	9.5e + 07 Pa	2.5e + 08 Pa

Table 10.2 Typical values of static and kinetic friction for different material combinations

Material combinations	Coefficients of static friction	Coefficients of kinetic friction
Steel–Steel	0.74	0.57
Steel–Aluminum	0.61	0.47
Steel–Teflon	0.04	0.04

as material of the frame. The material parameters are presented in Table 10.1. Additionally, the internal surface of the frame can be covered with extra lubricious shell. In the simulations, teflon (polytetrafluoroethylene—PTFE) was used as the material of extra lubricious shell. Teflon is one of the most heat-resistant synthetic materials (may operate in temperatures ranging from −200 °C to +260 °C) and has the lowest friction coefficient among all solids.

Static and kinetic coefficients of friction between two arbitrary materials are the measures of friction generated when they are in contact with each other. The friction coefficient usually varies between *0* for slippery objects and *1* for rough objects.

Typical values of static and kinetic friction coefficients for materials used in the model are presented in Table 10.2. The viscous friction between two movable surfaces depends on dimensional parameters, such as the contact area and the clearance between the two surfaces, and on fluid properties, e.g., specific gravity and viscosity. The clearances between the actuator and the frame are of the order of microns. In simulations of mechanical systems, in general, project developers often assume constant viscous friction in order to simplify the model. The value of the viscous friction coefficient for air and the clearance equal to 4 microns was equal to 0.05.

10.4 Model (1D) of RrVG System in LMS Imagine Lab AMESim

Cascade system simulations, performed in AMESim, were intended to fit and optimize the control system. The reaction time and the total deflection of the rod were analyzed depending on the assumed frictional force and the masses of the system elements. The cascade model of RrVG made in the LMS Imagine Lab AMESim is presented in Fig. 10.4.

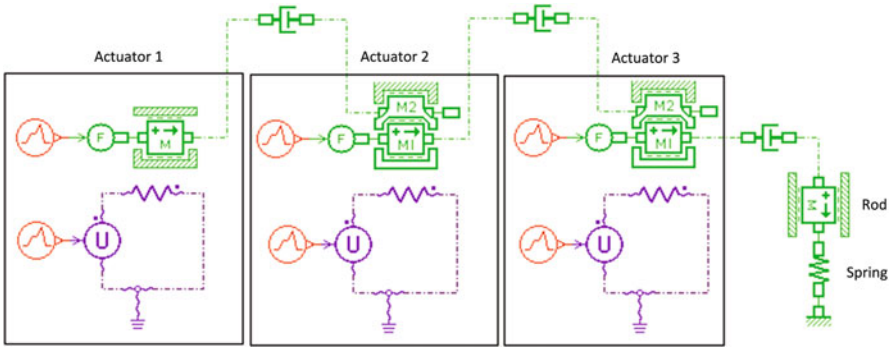

Fig. 10.4 RrVG – cascade model in Imagine Lab AMESim

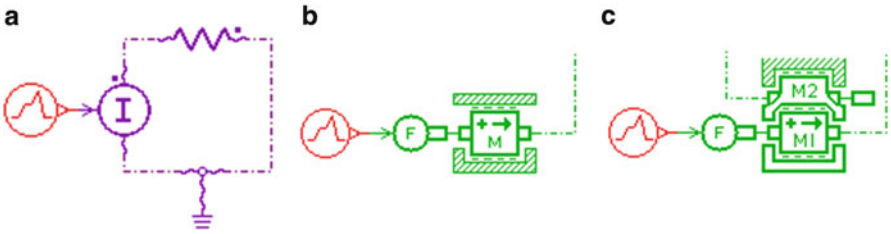

Fig. 10.5 Actuator – (**a**) electric part; (**b**) and (**c**) mechanical parts

The structures of all actuators are marked in the black rectangles. Each actuator consists of electrical and mechanical parts. These parts are shown in Fig. 10.5a. The electric part is represented by the resistance of the actuator, the voltage source, and the input signal submodel.

Depending on the location in the system, the mass submodels represent a single mass or combined masses. For the first actuator we have only the mass of the moving part of the actuator, because this actuator is permanently connected with the frame of the system. For other actuators, we have the sum of masses of the body of the actuator, the moving part, and the connector.

10.4.1 Description of Submodels

Input signal submodels are shown in Fig. 10.6. The element in Fig. 10.6a represents the linear signal source which can be used in electric and mechanical part. For electric part of actuator generated signal is shown in Fig. 10.3a, b but for mechanical part generated signal is shown in Fig. 10.3c.

The voltage source submodel is presented in Fig. 10.6b. The signal at port 3 controls the generated voltage on the output. Element from Fig. 10.6c converts a dimensionless signal input at port 1 to a force with the same value in N which is output at port 2.

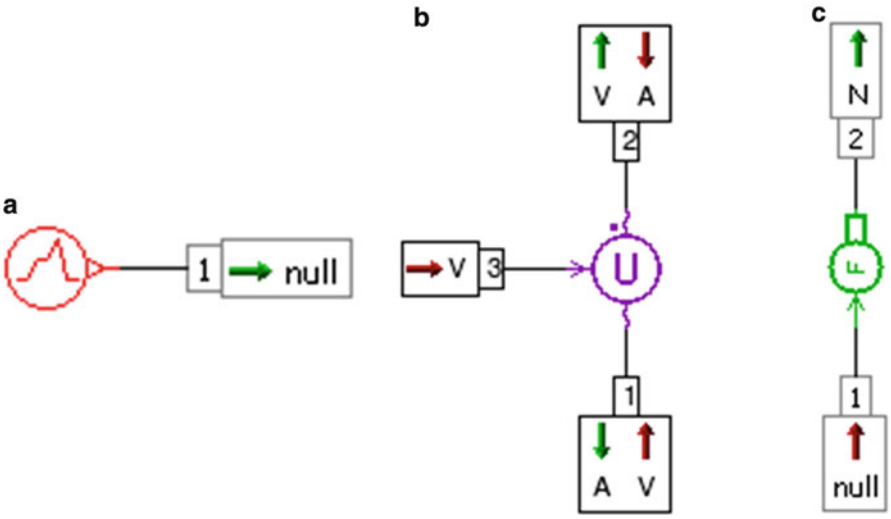

Fig. 10.6 Submodels of: (**a**) Signal source, (**b**) Voltage source, (**c**) Converter of signal

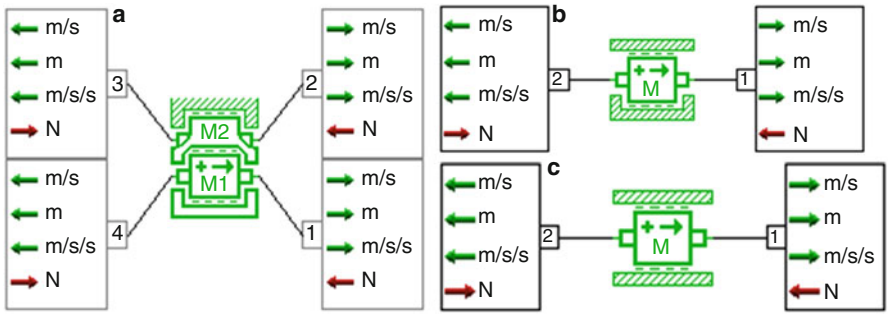

Fig. 10.7 Mass submodels

Mass submodels are presented in Fig. 10.7. Submodel in Fig. 10.7a represents the one-dimensional motion of two bodies under the action of external forces in *N* applied at four ports and frictional forces. One body, typically a slider, moves within the actuator body or whole actuator moves within the frame body. The displacements are limited to a specified range by inclusion of elastic end stops. In this submodel the mass M2 represents sum of mass body of the actuator outer body and connector. The friction force between the slider and the actuator body is modeled as Karnopp friction, stiction, Coulomb friction, viscous friction, and windage. Viscous friction and windage friction can be taken into account between the actuator and the frame body. In the cascade system, this type of mass submodel represents sum of the mass of actuator 2 and connector 1 and sum of the mass of actuator 3 and connector 2. The submodel in Fig. 10.7b

represents the one-dimensional motion of a two ports mass under the action of two external forces in N and frictional forces. The displacement is limited to a specified range by inclusion of ideal end stops. In the cascade system the submodel from Fig. 10.7b represents slider of actuator 1 which is fixed to the frame. The submodel in Fig. 10.7c represents the one-dimensional motion of a two ports mass under the action of two external forces in N and frictional forces. This mass submodel represents movable rod. All mass submodels return the velocity in m/s, the displacement in m, and the acceleration of the mass in m/s^2 for each body. For all mass submodels the inclination parameter allows for setting the inclination of the load in degrees, by the user. The friction characteristics are to be defined as follows: the coefficient of viscous friction in $N/(m/s)$; the coefficient of windage in $N/(m/s)^2$; the Coulomb friction force in N, and the stiction force in N. The windage is a force created on an object by friction when there is relative movement between air and the object. There are two possible causes of windage: the object is moving and being slowed by resistance from the air and a wind is blowing producing a force on the object. The windage force is approximately proportional to the square of the velocity. The friction coefficients between the actuator body and the slider have been set zero value because of the manufacturing specification (CEDRAT nd) of actuator there isn't information about.

Submodel in Fig. 10.8a represents an ideal mechanical spring. The submodel has two ports and gives force in N as outputs at both these ports. Connected submodels must provide velocities in m/s as inputs. The spring compression in m is calculated from the two displacement inputs. The geometrical and material parameters of the spring can be changed then the stiffness is computed using the expression for the helicoidal spring:

$$k = \frac{G \times d^4}{8 \times D^3 \times n_a} \pi r^2$$

where G is the material shear modulus N/m^2, n_a is the number of active coils, D is the spring diameter [mm], and d is the wire diameter [mm]. Submodels in Fig. 10.8b, c represent a damper with either a constant or variable damper rating and submodel a spring-damper which combines the features of these two elements. These are additional elements in order to match input and output parameters between successive elements of system. These elements are used to obtain the continuity of the model. In the real system a permanent connection between the slider and the connector (the slider and the rod) doesn't occur in this place.

10.4.2 Analysis and Results

As mentioned before, the damper or the damper-spring was used to obtain the continuity of the model which affects the system behavior. The geometrical and material parameters of the spring were as follows: $G = 8e + 07$ N/m^2, $n_a = 5$,

$D = 4.4$ mm, $d = 1$ mm. For these values the best result was obtained. Three positions of the system were analyzed:

– Case I: vertical position and the rod moving up,
– Case II: vertical position and the rod moving down,
– Case III: inclined position (angle 30°) and the rod moving up.

At the beginning the model was analyzed without load and friction forces in order to check the method of operation. Figure 10.9 shows displacements of cascade

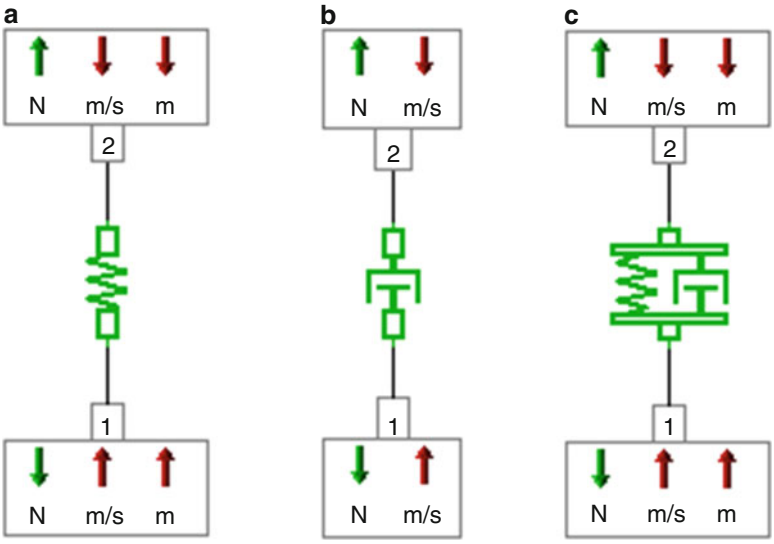

Fig. 10.8 Elements: (**a**) spring, (**b**) dumper, (**c**) spring-damper

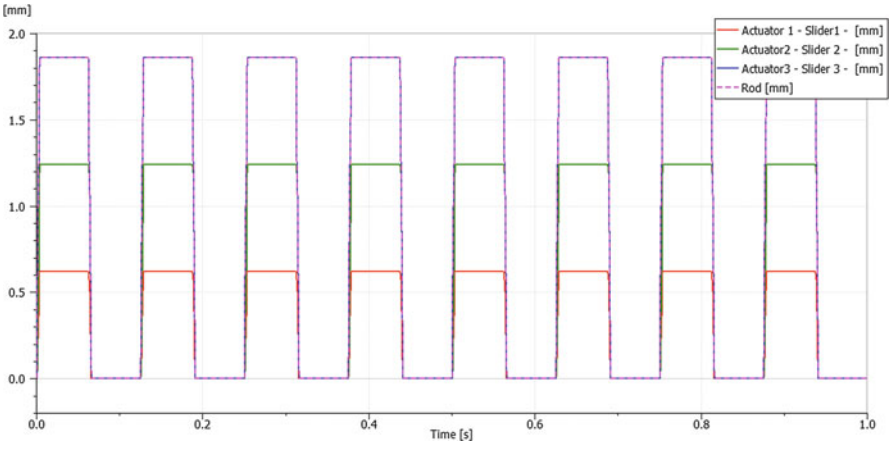

Fig. 10.9 AMESim – total displacements of sliders and rod – Case I

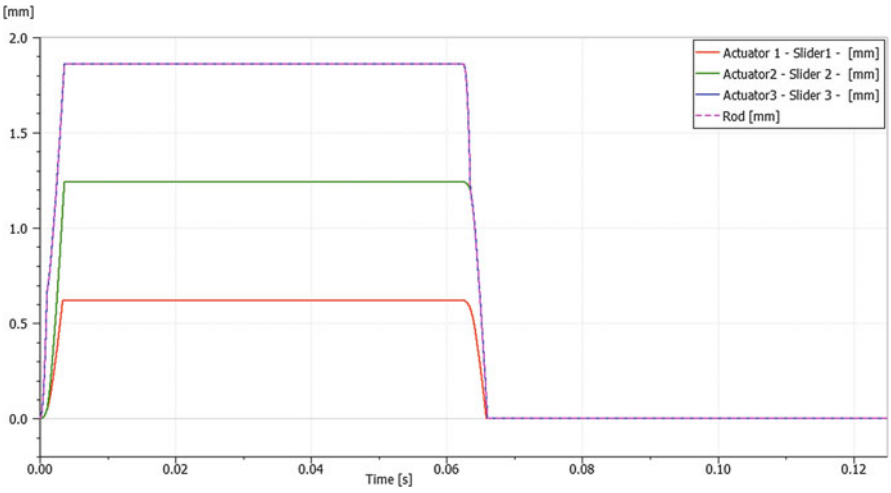

Fig. 10.10 AMESim – total displacements of sliders and rod – one period – Case I

elements as time functions for Case I. The displacements for Cases II and III look qualitatively similar, and certain differences appear only in the activation and returning times. From this figure we can see that the total displacements are consistent with the adopted assumption.

The displacement of a single slider is equal to about 0.62 mm and the sum of displacements of all sliders (displacement of the rod) is equal to 1.86 mm. The total displacement of the slider from Actuator 3 coincides with the displacement of the rod (purple line). Figure 10.10 presents one period of the signal from Fig. 10.9.

On the basis of that signal we can estimate the time of rod activation. The activation times (maximal times of rod displacement) are equal to 0.0041 s for Case I, 0.0038 s for Case II, and 0.004 s for Case III. The returning times are equal to 0.0035 s for Case I, 0.0037 s for Case II, and 0.0035 s for Case III. Since the system is analyzed without friction forces, we can assume that this is the minimum value of the rod activation time (Fig. 10.11).

The next step of the research was to use appropriate parameters of friction between the elements in order to obtain real behavior of the examined system. Figure 10.12 presents the ejecting and returning times for all cases with friction. The activation times are equal to 0.0047 s for Case I, 0.0044 s for Case II, and 0.0046 s for Case III. The returning times are equal 0.0038 s for Case I, 0.004 s for Case III, and 0.0038 s for Case III. We can see that the ejecting and returning times increased by about 15 % for the adopted/optimized friction coefficient values. On the basis of these graphs we can optimize the moment of activation and the delay time of an individual actuator.

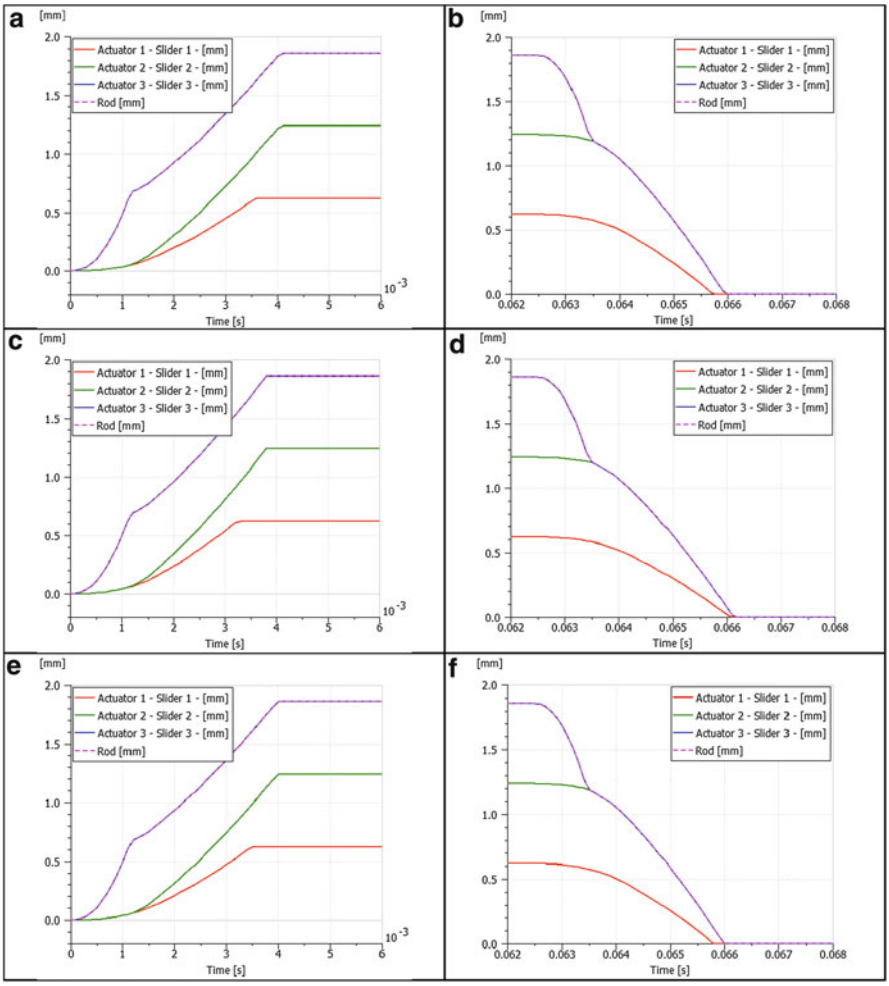

Fig. 10.11 AMESim – characteristics of ejection and return of the rod in time: (**a**, **b**) Case I, (**c**, **d**) Case II, and (**e**, **f**) Case III

10.5 Model (3D) of RrVG System in LMS Virtual Lab

The cascade model of RrVG was worked out in CATIA V5 environment integrated with LMS Virtual.Lab. The model is presented in Fig. 10.13. Starting with the geometry creation process, the bodies can be sketched, formed as solid geometries, assembled into a system of bodies, and connected by joints and forces.

The model is used both to predict loads and kinematic and dynamic behavior before the mechanical system is built, and to improve and troubleshoot the performance of the existing design. LMS Virtual.Lab offers a variety of analy-

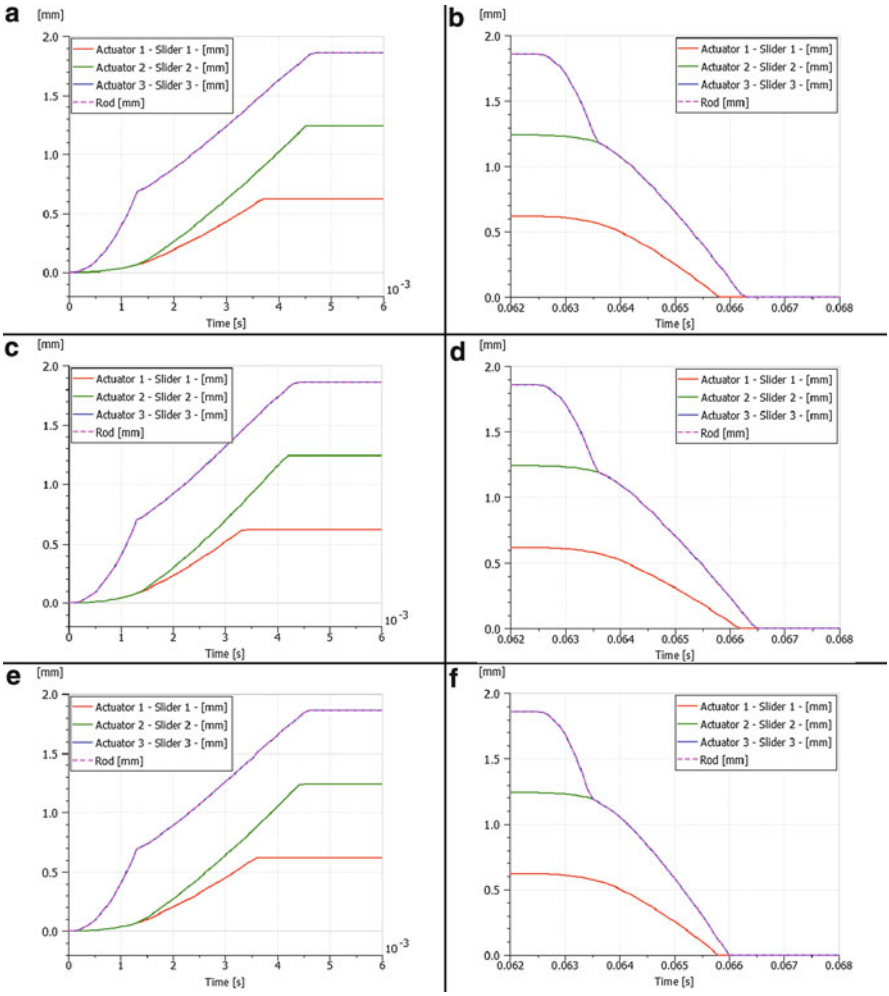

Fig. 10.12 AMESim – characteristics of ejection and return of the rod in time with friction: (**a**, **b**) Case I, (**c**, **d**) Case II and (**e**, **f**) Case III

sis types. Some types of analysis are performed sequentially. When models are first constructed, assembly analysis is run first to validate connectivity and accuracy of input. It is often useful to then run a static analysis of a dynamic system prior to running dynamic analysis to find the equilibrium position for all bodies. This ensures the dynamic run will be smooth and well behaved. Sometimes it is useful to run kinematic analysis to get body motion or path information for use in a subsequent dynamic run.

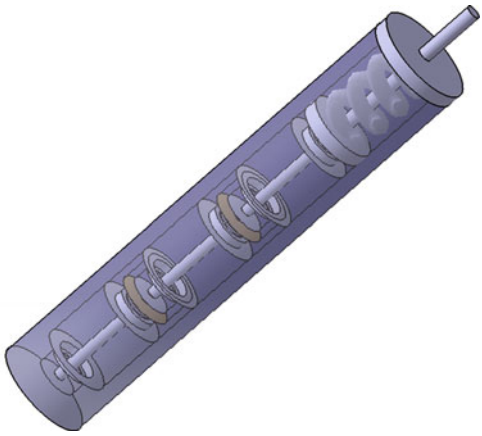

Fig. 10.13 Closed model of RrVG – cascade in LMS Virtual.Lab

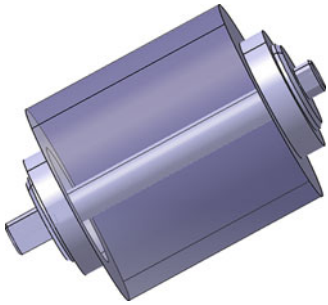

Fig. 10.14 The 3D model of BLMM actuator

10.5.1 Descriptions of Elements

The geometry and parameters (such as the mass, for instance) of the actuator were obtained from the manufacturer data (CEDRAT nd). The 3D model of the single actuator is presented in Fig. 10.14.

Figure 10.15 presents the connector and the movable rod. Figure 10.16 presents the frame with the lid of the system. Holes in the frame represent connections passing the control signal. The exact dimensions of the elements depend on the dimensions of the used actuator.

Table 10.3 presents the weights of individual elements based on the 3D model made in Virtual.Lab. The total mass of the cascade system is equal to 9.251 g (9.272 g with extra lubricious shell).

10.5.2 Kinematic Analysis

Kinematics deals with bodies connected by algebraic constraints and joints. The process of adding joints and constraints to the model involves selecting an element

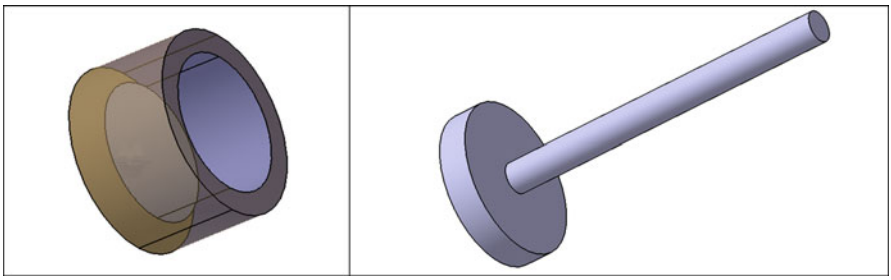

Fig. 10.15 The 3D model and characteristics of the connector and the movable rod

Fig. 10.16 The 3D model and characteristic of the frame and the frame lid

Table 10.3 Masses of elements and lubricious shell

Name of element	Material	Mass [g]
Outer body of actuator	Steel	1.024
Slider of actuator	–	0.076
Connector	Aluminum	0.088
Movable rod	Aluminum	0.079
Frame with lid	Steel	5.696
Lubricious shell	Teflon	0.021

type and picking the bodies and connection locations on the bodies. Joints define a relationship between two different bodies according to the kinematic constraints imposed by that type of joint. Each joint references geometric features on the two bodies connected by the joint. The joint also eliminates certain degrees of freedom that exist between the bodies connected by the joint. A cylindrical joint has been used between frame and movable elements in cascade. A constraint element defines a kinematic condition for one body or a relationship between two different bodies according to the type of kinematic constraint imposed. Constraints can be used to fix a point on a body to a specific location in global space, fix the distance between two points in global space, and fix the difference in the global coordinate of a point on each of the two bodies. Special constraints called drivers can be used

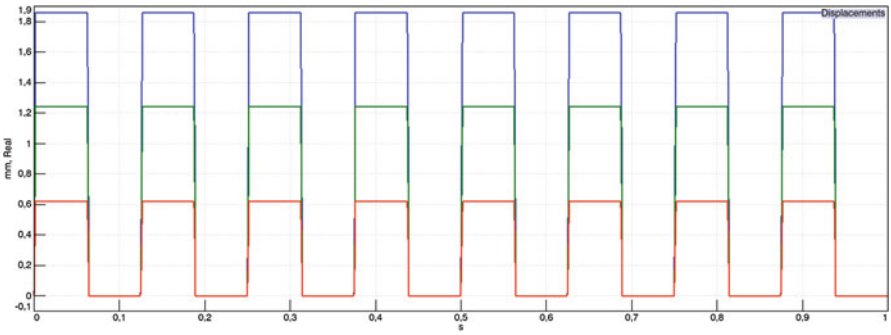

Fig. 10.17 Virtual.Lab – total displacements of sliders and rod – kinematic analysis

to define motion on a single body, between two bodies, or on a joint. Instead of a fixed constraint, these driver constraints are time varying constraints that allow you to exercise the free degrees of freedom of your mechanism. Defining a driver constraint in LMS Virtual.Lab consists of two basic steps. Step 1 is defining what you would like to drive, the position of a single body, a distance between two bodies, or a free degree of freedom on a joint. Step 2 is defining the actual driving function (Fig. 10.3d). A Joint Position Drivers were used in order to move actuator sliders and displacements of sliders respect to the frame. The initial results are presented in Fig. 10.17.

The red, green, and blue lines represent displacements of sliders for actuators 1, 2, and 3, respectively. The total displacements of the rod (purple line) coincide with the displacement of the slider from actuator 3. Analyzing the graph in Fig. 10.17 we can see that the masses and spring have no effect on the displacements. Figure 10.18 presents one period of the signal from Fig. 10.17.

Characteristics in Figs. 10.17 and 10.18 are analogical to the curves shown in Figs. 10.9 and 10.10. We can see that curves representing Virtual.Lab results are more straight than those representing AMESim results. This difference is caused by total absence of friction and connections between sliders and connectors. Additionally, the mass of the elements does not affect the movement of elements in the kinetic analysis (Fig. 10.19).

Therefore, the ejecting and returning times are equal to the commutation time (0.0017 s) of a single actuator. Results for all cases are the same for this type of analysis.

10.5.3 Dynamic Analysis

Dynamics deals with bodies, joints, and forces. The standard process of making a complete simulation involves defining the body locations and mass properties, followed by defining the constraints and kinematic joints connecting the bodies.

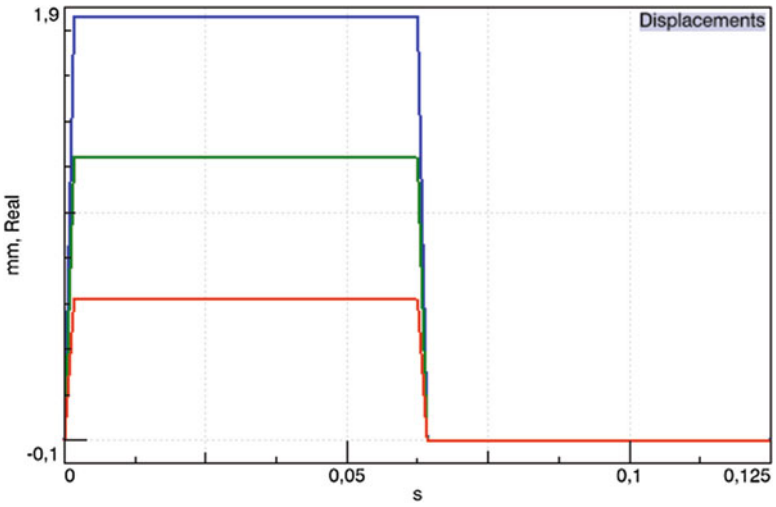

Fig. 10.18 VL – total displacements of sliders and rod – one period – kinematic analysis

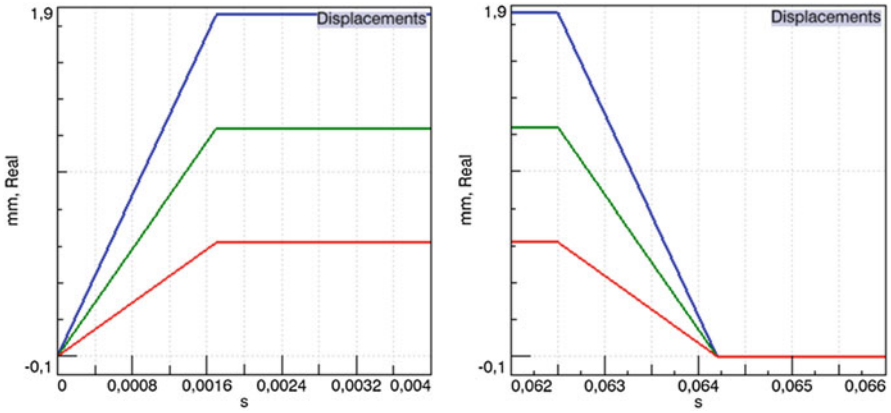

Fig. 10.19 VL – characteristics of ejection and return of the rod in time – kinematic analysis – Case I

Next, the dynamic force elements are specified. Most force elements act on one or two bodies and are a function of the position and velocity of connected bodies. Force elements do not remove any degrees of freedom from the equations of motion. They define the right-hand side terms in the equations of motion and affect the resulting body acceleration at each time step. Force elements also contribute to the solution in the case of static analysis, inverse dynamics, but not in kinematic analysis where forces are ignored. The following dynamic force elements have been specified. The Scalar Expression Force between the actuator body and the slider is applied in order to move the slider. This type of force is also used in order to add additional force as

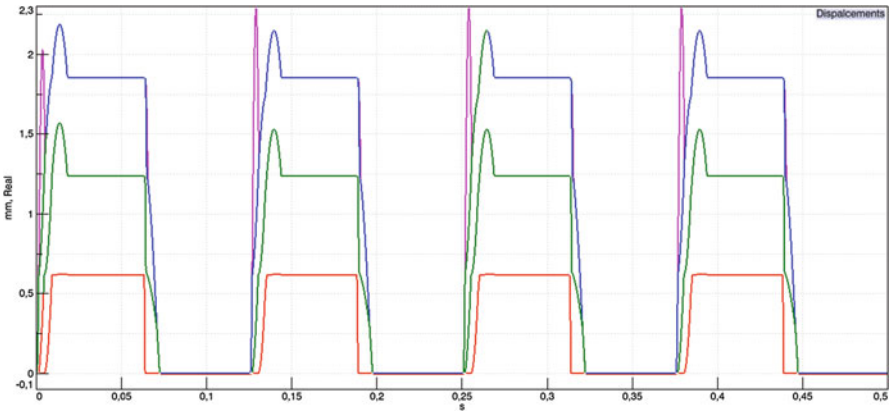

Fig. 10.20 VL – total displacements of sliders and rod – dynamic analysis Case I

the aerodynamic load. The Point-to-Point Contact force between sliders, connectors, and rod. The TSDA ("translational spring-damper-actuator") force between the base of rod and lid of frame. This force represents the main spring which is used in model. TSDA is also used to limit the maximum displacement of the slider with respect to the actuator body.

The initial results for the dynamic analysis without friction forces for Case I are presented in Fig. 10.20. The colors of the lines are the same as in the kinematic analysis. Purple line represents the displacement of the rod and partially coincides with the displacement of the slider from actuator 3. The influence of the reaction forces between the elements is significant. The application of TSDA as the endstop results in delays in actuator's response to the control signal. Therefore, the control signal required modification. Figure 10.21a, b presents the control signals for each actuator after modification, complemented by the dashed black line representing the initial control signal. The above-mentioned modifications consisted in changing the commutation time and shifting the control signal individually for each actuator. The distance between the following pulses activating the movement of the sliders was changed depending on which actuator was to be activated. Additionally, the control signals of actuators 2 and 3 were shifted in time.

Figure 10.22 presents the displacements of the sliders and the rod for the modified control signal. We can see that the displacement of the rod coincides with the displacement of the slider 3 from actuator 3.

Additionally, characteristic peaks appeared at the beginning of each period of displacement of an element. These peaks (short jumps of deflections) were not observed in the AMESim and kinematic results. Here, they appeared due to the fact that the system is discontinuous, and consecutive cascade elements are not permanently connected. The movement of the rod and actuators 2 and 3 is limited by the main spring which is applied in order to undo the rod. As was to be expected, the size and the shape of the peaks depend on the adopted parameters of the main spring.

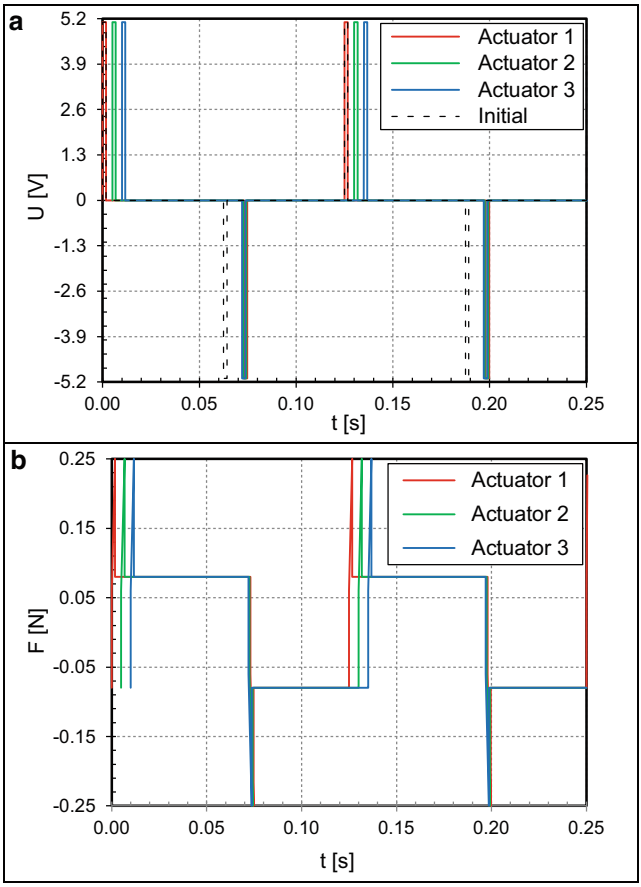

Fig. 10.21 Modified input and output signals for frequency 8 Hz, (**a**) voltage input signal and (**b**) force output signal

Spring performance is defined by such constant coefficients as: spring constant N/m, damping coefficient kg/s, and free length spring [m], defined in Virtual.Lab simulation. For excessively high values of the spring constant the rod will not be able to eject, while for very small values of the spring constant the returning time of rod is long. The damping coefficient tends to reduce the amplitude of oscillations in the system. The free length spring value defines the unreformed displacement of the spring. This value depends on the size of the system and is equal to 6.508 mm for all cases. For Case I with the modified control signal the spring constant is equal to 25 N/m and the damping coefficient is equal to 0.05 kg/s.

Each case was simulated for three different conditions: without friction force, with friction force, and with friction force and aerodynamic load of the rod. Figure 10.23a presents one period of total displacement of elements, the ejecting interval, and the returning interval from total displacement, for Case I without friction.

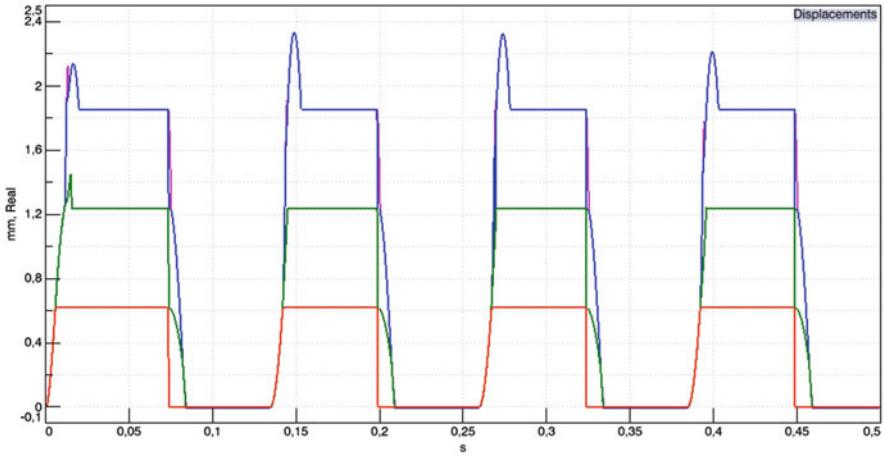

Fig. 10.22 VL – total displacements of sliders and rod after input signal modifications – dynamic analysis Case I

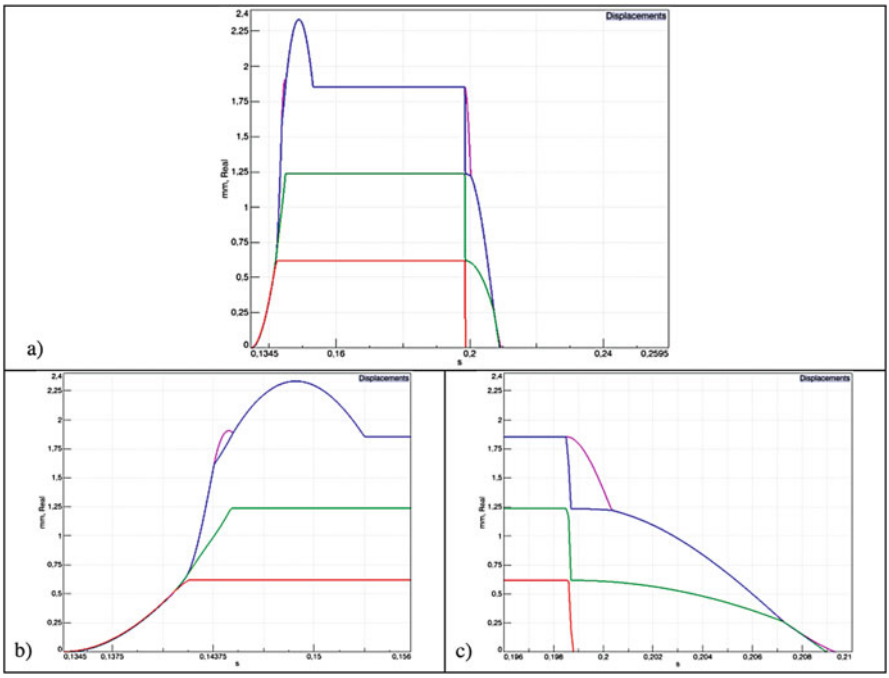

Fig. 10.23 VL – (**a**) Total displacements of sliders and rod – one period, (**b**, **c**) characteristics of ejection and return of the rod in time – Case I

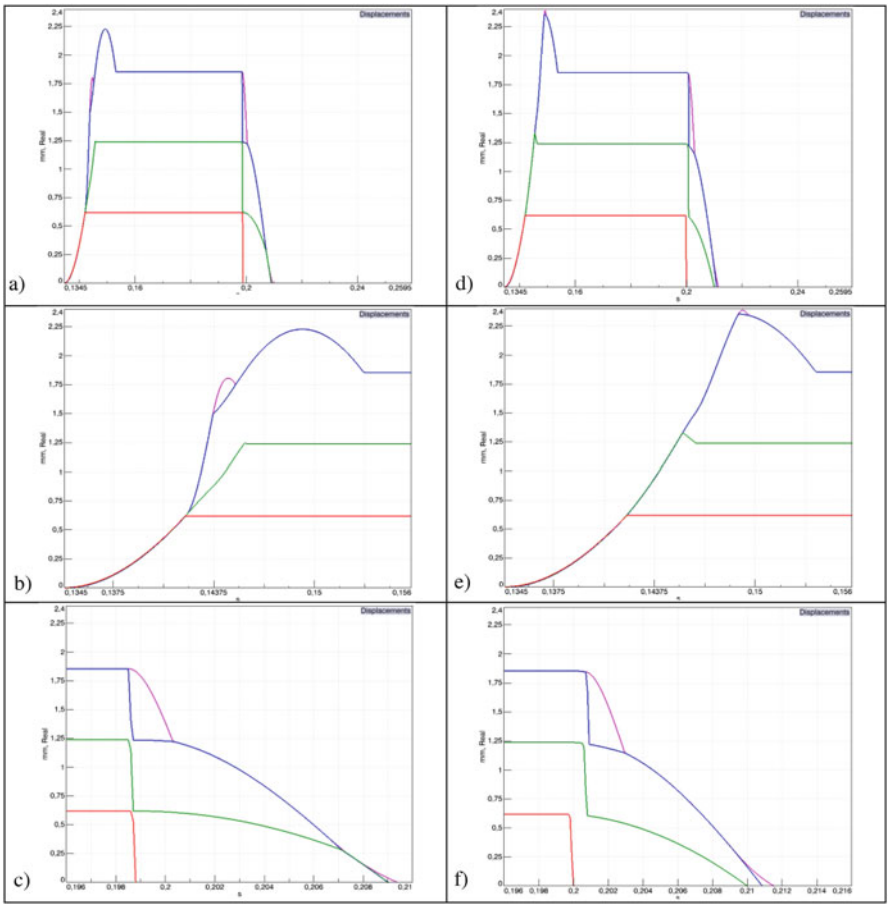

Fig. 10.24 VL – total displacements of sliders and rod, (**a–c**) characteristics of ejection and return of the rod in time – Case I – with friction; (**d–f**) Case I – with friction and aerodynamic load of rod

From Fig. 10.23b, c we can determine the ejecting and returning time of the rod to the operating deflection (≈1.86 mm). The eject time from the initial position of the rod up to the first moment when it achieves the operating displacement was examined. For comparison, the next figures present results for the same case but with additional friction force between the elements and aerodynamic load of the rod. Each friction element adds and removes constraints on the motion of the mechanism, therefore the number of degrees of freedom (DOF) varies as friction elements lock and unlock. Because Virtual.Lab searches for the time when locking and unlocking occurs, we may notice that the analysis is slower when these events occur.

Figure 10.24a–f presents results for Case I with friction force between the movable elements and the frame, and aerodynamic load of the rod. When the friction force was applied, the movement of the elements was slower. The aerodynamic load

Table 10.4 Ejection and return time of the rod, Case I

	Ejection time [s]	Return time [s]
Case I	0.00985	0.01075
Case I with friction	0.01115	0.01099
Case I with friction and aeroload	0.01296	0.01157

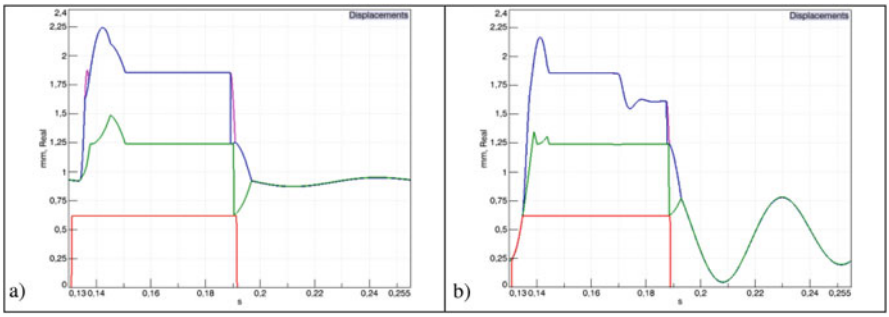

Fig. 10.25 VL – total displacements of sliders and rod – Case II for different constant spring values (**a**) 25 N/m (**b**) 50 N/m

of the rod was represented by an extra force applied to the tip of the rod. This force was changed depending on actual deflection of the rod. As a result, the observed movement of the rod was slower. The times of ejection and return of the rod for Case I are presented in Table 10.4.

For Case II, in which the system motion was reversed, the situation was completely different. It was necessary to change the control signal. Here, the initial control signal without modifications and offsets was used, see Fig. 10.3. Additionally, the parameters of the main spring were changed. Figure 10.25a presents displacement characteristics of the rod for the previous spring. We can see that the rod does not return to its initial position. Figure 10.25b presents the behavior of the system for the spring with strength enlarged by twice. For the stronger spring the system tries to return to the initial position but the displacement characteristics are deformed.

Therefore, the spring constant equal to 40 N/m was used for Case II. As a result, the system faster achieves the operating displacement, and the displacement characteristics are not deformed within the operating displacement range. However, the system does not return to its initial position and oscillates, see Fig. 10.26.

The times of ejection and return of the rod for Case II are presented in Table 10.5. The return times were undefined because the rod does not return to its initial position (Fig. 10.27).

The use of aerodynamic loads of the rod results in stronger interaction between the frame and the moving rod. For Case III (Figs. 10.28 and 10.29) the modified control signal was used (the same as in Case I) and the same the spring constant (Table 10.6).

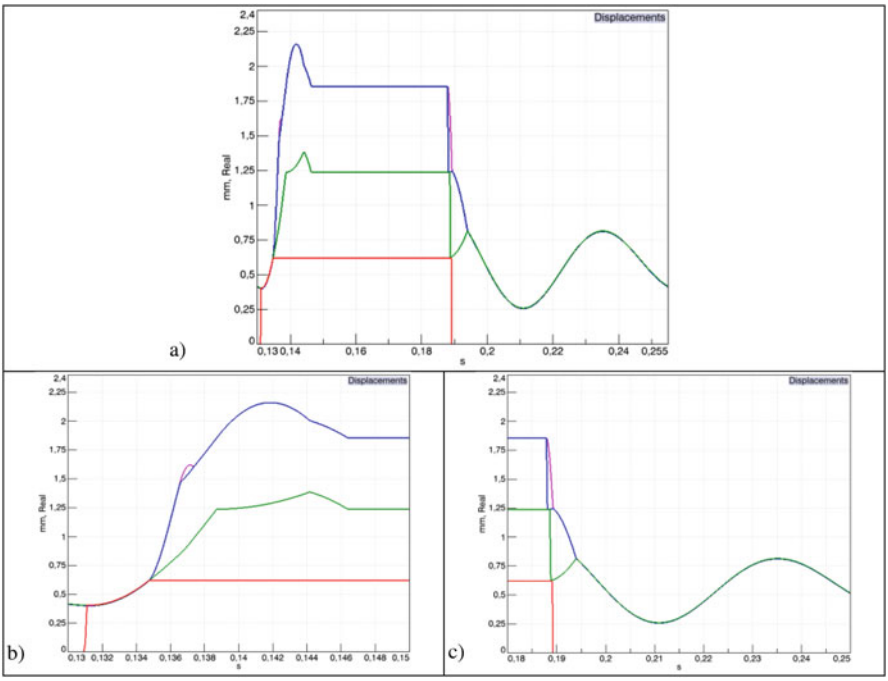

Fig. 10.26 VL – (**a**) Total displacements of sliders and rod – one period, (**b**, **c**) characteristics of ejection and return of the rod in time – Case II

Table 10.5 Ejection and return time of rod, Case II

	Ejection time [s]	Return time [s]
Case II	0.00783	undefined
Case I with friction	0.00788	undefined
Case I with friction and aeroload	0.00791	undefined

Table 10.6 Ejection and return time of rod, Case III

	Ejection time [s]	Return time [s]
Case III	0.01250	0.01275
Case III with friction	0.01261	0.01300
Case III with friction and aeroload	0.01290	0.01382

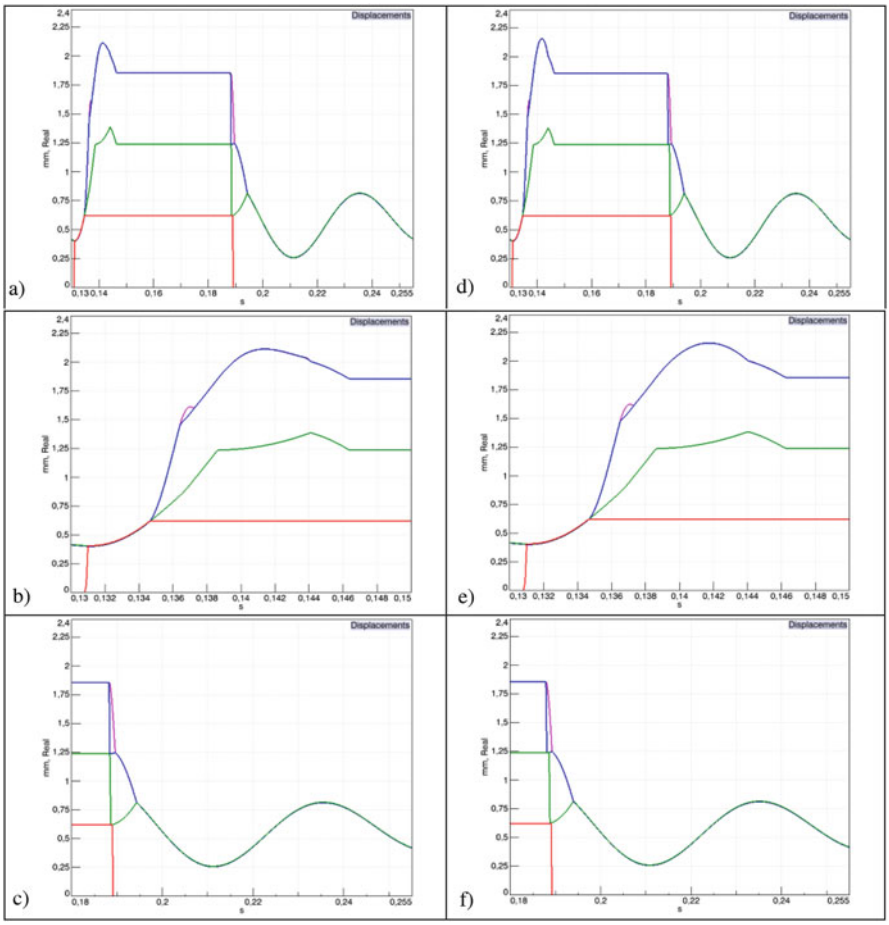

Fig. 10.27 VL – total displacements of sliders and rod, (**a–c**) – Case II with friction; (**d–f**) Case II with friction and aerodynamic load of rod

10.6 Conclusion

The main objective of the research was to build the Retractable rod Vortex Generator models using LMS software. The built models allow to analyze the system for various values of parameters. The one-dimensional model made in AMESim allowed preliminary simulation and analysis of the responses of individual moving parts. The three-dimensional model was made in VL. This model enables more realistic simulations of RrVG performance taking into account: loads of the rod, parameters of the friction force between the elements, position of the system

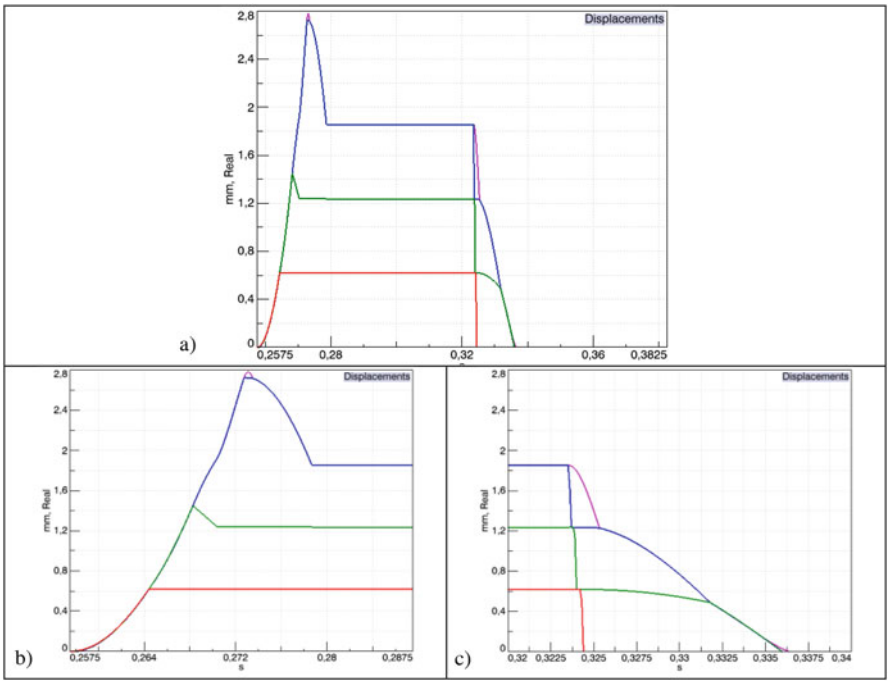

Fig. 10.28 VL – (**a**) Total displacements of sliders and rod – one period, (**b**, **c**) characteristics of ejection and return of the rod in time – Case III

(inclination angle), material of performance elements, and the optimized control signal. The simulation results showed the impact of the operation direction on system performance. Additionally, the change of the operation direction requires modification of parameters of individual elements (the main spring). When the system is directed down, the rod moves faster, but does not return to its original position. When typical materials (steel and aluminum) are used, the mass of the entire system is relatively low, which facilitates practical application. The simulations have shown that it is possible to obtain the time of rod ejection suitably shorter, as compared to the time of vortex generation (from the CFD results). In conclusion, the main objective of the research has been achieved.

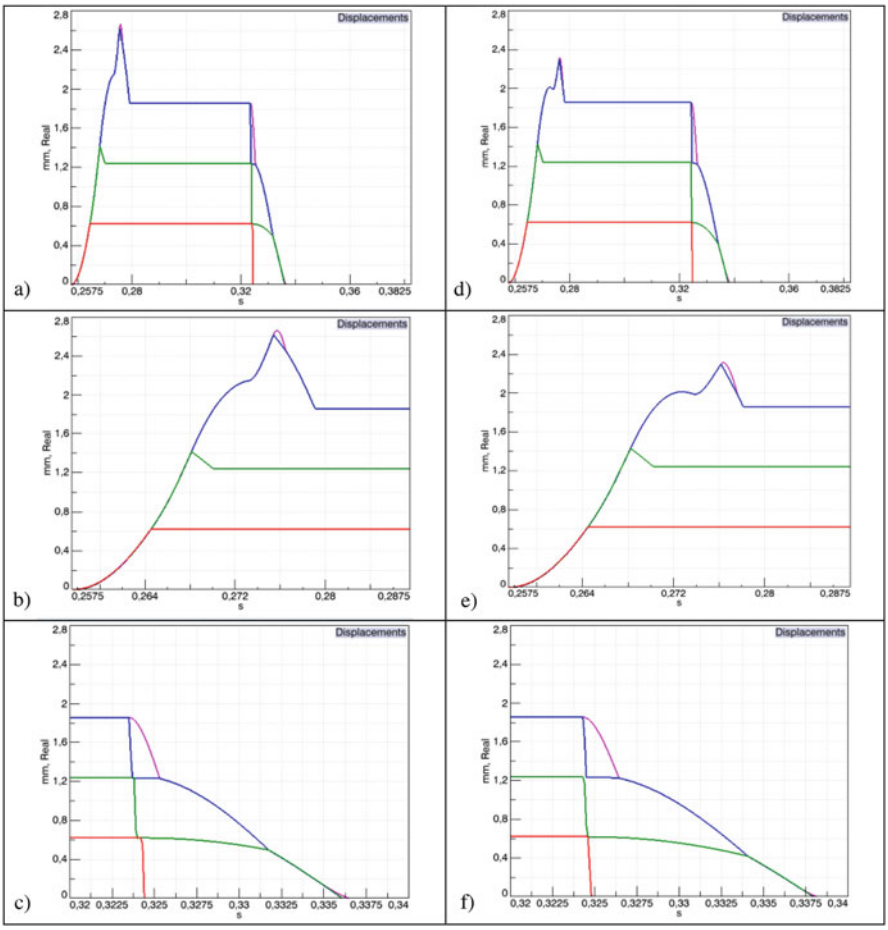

Fig. 10.29 VL – Total displacements of sliders and rod, (**a–c**) – Case III with friction; (**d–f**) Case III with friction and aerodynamic load of rod

References

Barakos G (2010) Bump at a Wall. In: Doerffer WP, Hirsch C, Dussauge J-P, Babinsky H, Barakos GN (eds) Unsteady effects of shock wave induced separation. Cambridge University Press, Cambridge, pp 13–53

CEDRAT (nd) Cedrat Technologies. Retrieved from Cedrat Technologies: http://www.cedrat-technologies.com/en/products/users-manual/actuators.html

Doerffer P, Szulc O (2011) Application of the passive control of shock wave to the reduction of high-speed impulsive noise. Int J Eng Syst Modell Simul 3:64

Flaszynski P, Tejero F (2013) RANS numerical simulation of effectiveness of vortex generators in a curved wall nozzle. IMP PAN

Pastrikakis V (2015) Flow control on helicopter rotors using active gurney flaps. PhD thesis, University of Liverpool

Siemens (nd) Siemens PLM Software. Retrieved from LMS Virtual.Lab: http://www.plm.automation.siemens.com/en_us/products/lms/virtual-lab/index.shtml

Siemens (nd) Siemens PLM Software. Retrieved from LMS Imagine.Lab Amesim: http://www.plm.automation.siemens.com/en_us/products/lms/imagine-lab/amesim/index.shtml

Tang H, Salunkhe P, Zheng Y, Du J, Wu Y (2014) On the use of synthetic jet actuator arrays for active flow separation control. Exp Therm Fluid Sci 57:1–10

Tejero F, Doerffer P, Szulc O (2014) Aerodynamic analysis of potential use of flow control devices. J Phys Conf Ser 530:012067